

# Theoretical understanding of LaTaON<sub>2</sub> decorated with metal cocatalysts for photocatalytic hydrogen evolution reaction

Xiang Zhang<sup>1</sup>, Yue Liu<sup>1</sup>, and Xin Zhou<sup>1</sup>

<sup>1</sup>Dalian University

January 09, 2025

## Abstract

LaTaON<sub>2</sub> is a promising visible-light-responsive photocatalyst for water splitting because of its broad visible light absorption and suitable band edge positions. However, the high defect concentration hinders the charge transfer and results in the poor photocatalytic performance of LaTaON<sub>2</sub>. Loading proper cocatalysts is one of the most efficient strategies for promoting charge separation/transfer and achieving high reaction activity. In this work, we have used density functional theory calculations to study the depositions of Pt, Ru and Ni single atom cocatalysts on LaTaON<sub>2</sub>(010) surface. The most stable adsorption configuration is the same site for all the elements, namely the top of the N atom on the La-terminated surface and the fourfold hollow site on the Ta-terminated surface. The adsorption of metal single atom on Ta-termination is stronger than that on La-termination due to the formation of more bonds. Upon the deposition, no localized impurity states appear in the middle of the forbidden gap since the *n d* states of metal adatoms are located within the valence band and conduction band of LaTaON<sub>2</sub>. The efficiency of the photocatalysts is probed by investigating their ability to adsorb H atom in a thermodynamically manner. Our results reveal that the energetically favorable sites of HER are the N atom on the La-termination and the O and N atoms on the Ta-termination, respectively. Compared with the clean surface, the surfaces with Pt, Ru and Ni single adatoms exhibit higher performance for HER because loading metal cocatalysts can further activate the surface nonmetal atoms and reduce the Gibbs free energy of hydrogen adsorption. The work gives an atom-level insight into the role of metal single atom cocatalysts in LaTaON<sub>2</sub> photocatalyst for hydrogen production.

## Theoretical understanding of LaTaON<sub>2</sub> decorated with metal cocatalysts for photocatalytic hydrogen evolution reaction

Xiang Zhang<sup>1</sup>, Yue Liu<sup>1</sup>, Xin Zhou<sup>1,2\*</sup>

<sup>1</sup> College of Environment and Chemical Engineering, Dalian University, Dalian, Liaoning 116622, P. R. China

<sup>2</sup> Interdisciplinary Research Center for Biology and Chemistry, Liaoning Normal University, Dalian, Liaoning 116029, P. R. China

\* Corresponding authors.

Email addresses: zhouxin@dlu.edu.cn

**Abstract:** LaTaON<sub>2</sub> is a promising visible-light-responsive photocatalyst for water splitting because of its broad visible light absorption and suitable band edge positions. However, the high defect concentration hinders the charge transfer and results in the poor photocatalytic performance of LaTaON<sub>2</sub>. Loading proper cocatalysts is one of the most efficient strategies for promoting charge separation/transfer and achieving high reaction activity. In this work, we have used density functional theory calculations to study the depositions of Pt, Ru and Ni single atom cocatalysts on LaTaON<sub>2</sub>(010) surface. The most stable adsorption configuration is the same site for all the elements, namely the top of the N atom on the La-terminated surface and the

fourfold hollow site on the Ta-terminated surface. The adsorption of metal single atom on Ta-termination is stronger than that on La-termination due to the formation of more bonds. Upon the deposition, no localized impurity states appear in the middle of the forbidden gap since the  $nd$  states of metal adatoms are located within the valence band and conduction band of LaTaON<sub>2</sub>. The efficiency of the photocatalysts is probed by investigating their ability to adsorb H atom in a thermodynamically manner. Our results reveal that the energetically favorable sites of HER are the N atom on the La-termination and the O and N atoms on the Ta-termination, respectively. Compared with the clean surface, the surfaces with Pt, Ru and Ni single adatoms exhibit higher performance for HER because loading metal cocatalysts can further activate the surface nonmetal atoms and reduce the Gibbs free energy of hydrogen adsorption. The work gives an atom-level insight into the role of metal single atom cocatalysts in LaTaON<sub>2</sub> photocatalyst for hydrogen production.

**Keywords** : photocatalysis; LaTaON<sub>2</sub>, metal cocatalysts; hydrogen evolution reaction; DFT calculations

## 1. Introduction

In recent years, hydrogen generation via photocatalytic water splitting based on heterogeneous photocatalysts has received much attention and become a promising strategy for solving the global energy crisis and environmental issues.<sup>1-4</sup> Most semiconductor-based photocatalysts with relatively high activity and excellent chemical stability are composed of transition metal oxides containing  $d^0$  and  $d^{10}$  metal ions. However, their large band gaps made them only active under the ultraviolet light irradiation, which makes up only a small part of the solar energy spectrum. Hence, in order to enhance the utilization of solar energy, extending the light absorption range of heterogeneous photocatalysts has become a hot research topic in this field. In this respect, the synthesis of perovskite-type transition metal oxynitrides with chemical formula AB(O,N)<sub>3</sub> (A=Ca, Sr, Ba, La; B=Ti, Nb, Ta) has drawn much attention, not only because they have photocatalytic activities under visible light irradiation caused by the higher energy level of N 2p than O 2p at the valence band maximum (VBM), but also because they can accomplish the overall water splitting reaction in principle due to their suitable band positions relative to the oxidation and reduction potentials of water.<sup>5-9</sup>

In the family of perovskite oxynitrides, LaTaON<sub>2</sub> is an attractive photocatalyst for splitting water because of its broad absorption in the visible light region and suitable band edge positions.<sup>10-14</sup> LaTaON<sub>2</sub> generally exhibits poor photocatalytic activity due to its high defect concentration and grain boundaries. To enhance the photocatalytic activity, various strategies were used in the LaTaON<sub>2</sub>-based materials, such as doping metals, loading suitable cocatalysts, and forming solid solutions or heterojunctions.<sup>15-22</sup> In 2006, Liu *et al.* found that LaTaON<sub>2</sub> with Pt or Ru as a cocatalyst showed high activity for reduction of water to H<sub>2</sub> in the presence of ethanol as a sacrificial electron reagent.<sup>23</sup> A remarkable enhancement in production efficiency was observed when both Pt and Ru were present. Zhang *et al.* observed the progress of H<sub>2</sub> evolution from an aqueous methanol solution over Pt-loaded LaTaON<sub>2</sub> flux under visible-light irradiation.<sup>24</sup> In 2017, Si *et al.* investigated the behavior of different cocatalyst on LaTaON<sub>2</sub> photoanode for decomposing water.<sup>25</sup> Their results showed that Ni-based oxides lead to higher improvement than other oxidation cocatalysts on the photoelectrochemical performance, and severe recombination of photogenerated carriers in bulk or poor electronic conductivity may be main factors limiting the photon-to-current conversion efficiency in LaTaON<sub>2</sub> photoanodes. Hojamberdiev *et al.* found that with Pt and CoO<sub>x</sub> as cocatalysts, LaTaON<sub>2</sub> showed higher photocatalytic activities and photoanodic response of HER and OER than PrTaON<sub>2</sub> mainly due to a less amount of intrinsic defects and reduced tantalum species.<sup>26</sup> In 2018, Huang *et al.* reported that after the modification of CoO<sub>x</sub>, the solar photocurrent of LaTaON<sub>2</sub> was an order of magnitude larger than the previously-reported value, which primarily resulted from bulk defect control and interface engineering.<sup>27</sup> In 2019, Wang *et al.* synthesized facet-controlled LaTaON<sub>2</sub> with low defect concentrations through selecting LaKNaTaO<sub>5</sub> as the appropriate oxide precursors, which exhibited the photocatalytic activity of HER four times greater than that obtained from the samples modified with a Rh cocatalyst.<sup>28</sup> In 2022, Xu *et al.* synthesized a platy LaTaON<sub>2</sub> by a one-pot nitridation route, which showed a six-fold increase in photocatalytic H<sub>2</sub> evolution activity compared with the conventional LaTaON<sub>2</sub> powder after loading with a Pt cocatalyst.<sup>29</sup> In the visible-light-driven Z-scheme overall water splitting system, Pt/LaTaON<sub>2</sub> served as

H<sub>2</sub>-evolving photocatalyst.

As can be seen, metal cocatalysts are essential components in LaTaON<sub>2</sub> photocatalytic system for highly efficient hydrogen production since they are beneficial to promoting the separation/transfer of photoinduced carriers and reducing the reaction energy barrier.<sup>30</sup> However, some critical questions about cocatalysts still need to be addressed, such as the stable location of cocatalysts on the semiconductor surface, the effect of loading cocatalysts on the electronic structure, the relationship between the type of cocatalysts and the reaction activity, and so on. The structural complexity of nanoscale cocatalysts makes it difficult to obtain the relevant information above in experiments. In this respect, density functional theory (DFT) calculations have been proven to be a favorable supplement to experimental measurements in revealing the structure-property relationship and reaction mechanism of various photocatalytic systems.<sup>31, 32</sup> In this work, we have theoretically simulated LaTaON<sub>2</sub> loaded with metal (M) cocatalysts (M=Pt, Ru and Ni) presenting as a single atom.<sup>33, 34</sup> We have constructed different surface terminations based on the relative stable structure of bulk LaTaON<sub>2</sub>, searched the most stable adsorption site of metal cocatalysts, studied the electronic structures of photocatalytic systems and the mechanism of HER, and explored the role of cocatalysts in influencing the reaction activity.

### Computational methods

Spin-polarized DFT calculations were carried out by utilizing the projected augmented wave method implemented in the Vienna ab initio simulation package.<sup>35-38</sup> The valence electrons were expanded into a set of plane waves with a cutoff of 450 eV. The Perdew-Burke-Ernzerhof (PBE) functional under the generalized gradient approximation was applied to represent the exchange-correlation potential.<sup>39, 40</sup> The convergence criterion of electronic and ionic loops were set to be 10<sup>-4</sup> eV and 10<sup>-2</sup> eV/Å, respectively. According to the experimental measurements in literatures,<sup>41, 42</sup> we chose the orthorhombic crystal structure with the space group *Imma* to model bulk LaTaON<sub>2</sub>. There are 20 atoms in the unit cell with the lattice parameters of  $a = 5.716$  Å,  $b = 8.067$  Å,  $c = 5.746$  Å, and  $\alpha = \beta = \gamma = 90^\circ$ . A 7×5×7 Monkhorst-Pack  $k$ -point sampling was used to calculate the structural and electronic properties of bulk. The PBE +  $U$  method was utilized to calculate the electronic properties, in which only the difference  $U_{eff}$  between the exchange  $J$  and Coulomb  $U$  parameters was considered. Here, we used a  $U_{eff}$  value of 5 eV for Ta 5d orbitals to obtain the similar band character to experimental measures.<sup>22, 26, 42</sup>

Stoichiometric slab models containing even atomic layers were constructed for simulating the low-index surfaces of bulk LaTaON<sub>2</sub>. In the perpendicular direction to each surface, a vacuum layer of 15 Å was added to eliminate spurious interactions between periodic images. The dipole correction was used in calculations to compensate the depolarizing field resulting from the asymmetry of the slab. The surface energy was computed to evaluate the stability of surface terminations with Monkhorst-Pack  $k$ -point samplings of 5×7×1 for (100), 7×7×1 for (010) and 7×5×1 for (001), respectively. To model the (2×2) supercell with adsorbates, the atoms in the bottom two layers were fixed at bulk positions and other parts were fully relaxed, and a 3×3×1  $k$ -point mesh was applied to perform the structural relaxation and self-consistent calculations.

## 3. Results and discussion

### 3.1. Bulk ordering and electronic structure

Anion ordering in oxynitride perovskites has long been the focus of research in the field.<sup>43-46</sup> The experimental investigation on LaTaON<sub>2</sub> by high resolution powder neutron and electron diffraction proposed that the *cis* configuration is energetically favored, in which the two O atoms in the same TaO<sub>2</sub>N<sub>4</sub> octahedron occupying the two adjacent edge positions.<sup>47</sup> Accordingly, we have constructed six configurations with *cis*-ordering for bulk LaTaON<sub>2</sub>.<sup>48</sup> The relaxed structures are presented in Figure 1. The structure **e** is calculated to be the most stable, which is 0.30 eV, 0.33 eV, 0.09 eV, 0.06 eV, and 0.44 eV lower than **a**, **b**, **c**, **d**, and **f**, respectively. The calculated lattice parameters of structure **e** are  $a = 5.727$  Å,  $b = 8.032$  Å,  $c = 5.747$  Å, and  $\alpha = \beta = \gamma = 90^\circ$ , which are in good agreement with experimental values. Hence, we only use **e** configuration to model the bulk structure of LaTaON<sub>2</sub> and carry out the following calculations. Band structure along high-symmetry points in the Brillouin zone and density of states (DOS) are calculated by PBE+U method

and summarized in Figure 2. The results demonstrate that LaTaON<sub>2</sub> is an indirect semiconductor with the VBM at *D* point and the conduction band minimum (CBM) at  $\Gamma$  point, and the band gap is 2.15 eV, which are consistent with the experiments.<sup>22, 26, 42</sup> DOS and electron cloud distributions of frontier orbitals demonstrate that the VBM is mainly composed of N 2p states, and the CBM dominantly consists of Ta 5d states. La 6s states have little contribution to the VBM and CBM.

### 3.2. Adsorption of metal single atom on the surface of LaTaON<sub>2</sub>

Based on the relaxed bulk structure, (100), (010) and (001) surfaces are built using (1×1) sized periodic slabs including eight atomic layers. The computed surface energies are 2.24 m/Å<sup>2</sup> for (100), 1.46 m/Å<sup>2</sup> for (010) and 2.12 m/Å<sup>2</sup> for (001). The smaller the surface energy, the more stable the surface. As can be found, the stability of (010) is notably higher than other two surfaces. Hence, (010) surface is chosen to act as the support for loading the metal cocatalysts. As shown in Fig. 3, there are two possible terminations exposed with La and Ta atoms for (010) surface of LaTaON<sub>2</sub>, which are named as La-termination and Ta-termination, respectively. To find the stability tendency of metal single atom cocatalysts on the surface, we initially consider seven adsorption sites on the La-termination and eight adsorption sites on the Ta-termination, as displayed in Fig. S1. After the optimization, some initial structures undergo important displacement-relaxation procedure. Consequently, three and four stable adsorption sites are found on La-termination and Ta-termination, respectively, which are highlighted in Fig. 3. The relative energies of varied adsorption structures are suggested in Fig. 4. For La-termination, all the studied metal single atoms preferentially adsorb on the site of top<sup>N</sup>. While for Ta-termination, the most stable adsorption site for all the metals is located above the La atom in the sublayer, hollow<sup>La</sup>.

The adsorption energy is computed for the most stable structure of each metal adatom on LaTaON<sub>2</sub> (010) surface by Equation (1):<sup>49</sup>

$$E_{\text{ads}} = E_{M@ \text{ surface}} - E_{\text{ surface}} - E_{\text{ M}} \quad (1)$$

where  $E_{M@ \text{ surface}}$ ,  $E_{\text{ surface}}$ , and  $E_{\text{ M}}$  represent the energy of a surface adsorbed with metal single atom, the energy of a clean surface and the energy of a free metal atom, respectively. Based on the definition, the more negative the adsorption energy, the more stable the structure. The most stable structures and the corresponding adsorption energies are presented in Fig. 5, and the less stable structures are shown in Fig. S2. The La- and Ta-termination attached with Pt, Ru and Ni adatom are denoted as Pt@La, Ru@La, Ni@La, Pt@Ta, Ru@Ta and Ni@Ta, respectively. As can be seen from Fig. 5, the adsorption energies are in the range from -7.10 eV to -3.48 eV, which reveal that there are strong interactions between metal adatoms and the surface terminations. For the same termination, the adsorption of Ru on the surface is the strongest, followed by Pt and Ni. The adsorption of a metal atom on Ta-termination is stronger than that on La-termination, which is mainly due to the formation of more new metal-nonmetal bonds in the former.

*The adsorption of single metal atoms leads to the deformation of local structures, especially the displacement of the atoms in the top two layers. For La-termination, the predicted bond lengths are 1.937 Å for Pt-N, 1.783 Å for Ru-N, 1.737 Å for Ni-N, which become smaller with the increase in the number of valence electrons layers of metal adatoms.* The adsorption of the metal atom causes the N atom right below it to move upwards. The calculated N-Ta bond lengths are 2.089 Å in Pt@La, 2.080 Å in Ru@La and 2.070 Å in Ni@La, longer than 1.969 Å in pure La-termination. For Ta-termination, the metal adsorbate forms four covalent bonds with the adjacent nonmetal atoms in each case. The bond lengths of M-O are 2.088 Å in Pt@Ta, 2.154 Å in Ru@Ta and 1.936 Å in Ni@Ta. The average distances of M-N bonds are 2.085 Å in Pt@Ta, 1.973 Å in Ru@Ta and 1.945 Å in Ni@Ta. Two Ta atoms neighboring to the metal adatom move to the inner of the surface due to Coulomb repulsion between them. It turns out that the bond lengths between the Ta atom and the sublayer O atom are computed to be 1.945 Å in Pt@Ta, 1.940 Å in Ru@Ta and 1.944 Å in Ni@Ta, which are shorter than that in pure Ta-termination (1.953 Å).

To study the influence of metal adsorption on electronic structures of LaTaON<sub>2</sub> surface, we have calculated DOS of each adsorption structure and exhibited the partial density of states (PDOS) for La 5*d*, Ta 5*d*, O 2*p*, N 2*p* and M *nd* states in Fig. 6. For all of six systems, the VBM is primarily composed of N

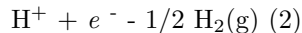
2p states and the CBM mostly consists of Ta 5d states, which are similar with the band features of bulk. The adsorption of metal single atoms does not cause any impurity states in the forbidden gap, which can become the recombination center of photogenerated electrons and holes, and are adverse to the enhancement of photocatalytic activity. The majority of Pt 5d, Ru 4d and Ni 3d states are located in the lower energy region of the VBM and the minor of them are located in the top of the VBM or the CBM.

*The Bader charge analyses show that the effective charges of adatoms are -0.74 e for Pt@La, -0.57 e for Ru@La, -0.45 e for Ni@La, 0.24 e for Pt@Ta, 0.82 e for Ru@Ta and 0.56 e for Ni@Ta. These results reveal that the metal adatoms receive electrons from La-termination while they lose electrons to Ta-termination. The remarkable difference in the direction of the charge transfer between the adatom and the surface can be explained by that the larger negative charges of the nitrogen (by 0.17 e) and oxygen atoms (by 0.20 e) on La-terminated surface than Ta-terminated surface results in a poorer oxidizing ability in the former than in the latter.<sup>50</sup> The charge redistribution at the interface between the adatom and LaTaON<sub>2</sub> surface are visualized by the charge density difference in Fig. 7, where the yellow and cyan contours represent the accumulation and depletion of charge densities, respectively. M@La (M=Pt, Ru and Ni) systems demonstrate the similar character, that is, the attachment of metal single atoms mostly promotes the localized changes in the charge densities of metal adatom and the connected N atom, which is reified as the transfer of charge density from the N atom to the metal adatom. The redistribution of charge is found to be more delocalized in M@Ta than in M@La (M=Pt, Ru and Ni) since the embedded metal atom forms more bonds in the former than in the latter. As to all the M@Ta (M=Pt, Ru and Ni) systems, a large area of the charge depletion appears around the metal adatom and the charge accumulation region are mainly located at the neighboring nonmetal atoms. The direction of charge transfer is consistent with the prediction of Bader charge.*

Work function is the required energy of removing one electron from the Fermi level to the vacuum level, which plays an important role in the charge transfer and the band bending in the interfacial structure. To explore the effect of adsorbing metal single atoms on the work function of LaTaON<sub>2</sub> (010) surface, we have calculated the difference of work functions between the surface with an adsorbate and the pristine surface ( $\Delta\Phi$ ). A positive value indicates that the work function of the surface adsorbed with a metal atom is larger than that of the pristine surface. The predicted values of  $\Delta\Phi$  are 0.15 eV for Pt@La, 0.10 eV for Ru@La, 0.06 eV for Ni@La, -0.03 eV for Pt@Ta, -0.04 eV for Ru@Ta, -0.05 eV for Ni@Ta. Our results demonstrate that depositing metal atoms on different termination of LaTaON<sub>2</sub> can slightly tune the work function of the photocatalytic system. Loading metal single atoms on Ta-terminated surface leads to the decrease of work function, which is favorable to the escape of electrons from the surface of semiconductor.

### 3.3. Hydrogen evolution reaction mechanism

In the photocatalytic reactions, loading proper metal cocatalysts is one of the most effective methods of enhancing the HER performance since they can act as the reactive sites, promote the charge separation and decrease the reaction barrier.<sup>30</sup> In the present work, we only focus on the thermodynamic process of the surface reaction. HER is generally considered to be a three-state process and can be described by the following equation:



The Gibbs free energy of the initial state is equal to that of the final state under the standard electrode voltage.<sup>51</sup> Thus, the catalytic activity of HER is mainly correlated with the Gibbs free energy change ( $\Delta G_{\text{H}}$ ) of the process from the initial state to the adsorptive state, which can be calculated based on Equation (3):<sup>52</sup>

$$\Delta G_{\text{H}} = \Delta E_{\text{H}} + \Delta ZPE - T \Delta S_{\text{H}} \quad (3)$$

where  $\Delta E_{\text{H}}$  is the adsorption energy of a H atom attached to the active site of the surface,  $\Delta ZPE$  is the difference in the zero-point energies of an adsorbed species and a gaseous phase, and  $\Delta S_{\text{H}}$  is equal to the negative value of half the entropy of H<sub>2</sub> in the gas phase under the standard conditions.<sup>53</sup> The more positive the value of  $\Delta G_{\text{H}}$ , the more difficult the adsorption of the H atom on the surface. While the more negative the value of  $\Delta G_{\text{H}}$ , the more difficult the desorption of H<sub>2</sub> from the surface. Hence,  $\Delta G_{\text{H}}$  should be close to

zero for the ideal catalyst of HER.<sup>54</sup>

For both terminations of clean surface, M@La and M@Ta systems (M=Pt, Ru and Ni), we have examined possible adsorption sites of hydrogen, including the exposed La, Ta, O, N and metal adatoms. The optimized structures are summarized in Fig. 8 and the corresponding values of  $\Delta G_{\text{H}}$  are utilized to draw the free-energy diagram of HER. As we know, the ideal catalyst for the HER is regarded as  $\Delta G_{\text{H}}=0$ , since both adsorption and desorption steps are thermoneutral.<sup>55</sup> In other words, the closer  $|\Delta G_{\text{H}}|$  is to zero, the better the catalysts. As shown in Fig. 8(a), for pure BaO-termination, the calculated values of  $\Delta G_{\text{H}}$  are 0.36 eV at the N site, 0.84 eV at the La site and 1.28 eV at the O site, which indicate that the hydrogen adsorption on this termination is endergonic and the N site is more active than metal sites in the HER. For pure TaON-termination, the calculated values of  $\Delta G_{\text{H}}$  are -0.63 eV at the N site, -0.60 eV at the O site and 1.78 eV at the Ta site, which suggest that the hydrogen adsorptions on the nonmetal atoms is energetically much more favorable than that on the Ta atom.

Fig. 8(b), 8(c) and 8(d) illuminate that the calculated values of  $\Delta G_{\text{H}}$  varies in the site of hydrogen adsorption, ranging from -0.77 to 0.99 eV for Pt@La, from -0.17 to 1.01 eV for Pt@Ta, from -0.77 to 0.89 eV for Ru@La, from -0.18 to 1.12 eV for Ru@Ta, from -0.68 to 0.84 eV for Ni@La, and from -0.05 to 0.99 eV for Ni@Ta. For M@La (M=Pt, Ru and Ni), the value of  $\Delta G_{\text{H}}$  at the N site is remarkably closer to zero than those at other sites, which shows that the N site is the most active site in the HER. The adsorption of hydrogen on the metal adatom is quite stable since the values of  $\Delta G_{\text{H}}$  are -0.68 eV for Ni@La and -0.77 eV for both Pt@La and Ru@La. The strong adsorption is unfavorable to the following desorption step. The hydrogen adsorptions on the O atom and La atom are relatively difficult since the process is endergonic. As to M@Ta (M=Pt, Ru and Ni), both the N and O atoms binding to the metal adatom can be the active sites of HER since the computed values of  $|\Delta G_{\text{H}}|$  at two sites are comparable and closer to zero than those at other sites. The adsorption of hydrogen on the metal adatom and La atom is energetically unfavorable due the larger positive values of  $\Delta G_{\text{H}}$ . Our results demonstrate that the active sites of HER are the exposed nonmetal atoms on the surfaces with and without single metal adatoms. The adsorption of Pt, Ru and Ni single atom on the LaTaON<sub>2</sub> (010) surface activates the adjacent nonmetal atoms and significantly decreases the value of  $|\Delta G_{\text{H}}|$ .

#### 4. Conclusions

In this work, DFT calculations have been performed to explore the most stable configuration, density of states, charge transfer, work function and HER performance of Pt, Ru and Ni single atoms supported on the (010) surface of LaTaON<sub>2</sub> to understand the effect of metal cocatalysts on the substrate properties. Our results reveal that all the metal adatoms prefer the top<sup>N</sup> site on the La-termination and the hollow<sup>La</sup> site on the Ta-termination. The interaction between metal adatoms and substrate is stronger on the Ta-termination than the La-termination because of the formation of more covalent bonds in the former. PDOS curves suggest that *nd* states of metal adatoms are well mixed with the VBM and CBM of semiconductor surface, which guarantees no impurity states in the middle of the band gap. This can avoid the formation of recombination center of photoinduced charge carriers. The adsorption of Pt, Ru and Ni single atoms slightly increase the work function of La-terminated surface and decrease the work function of Ta-terminated surface, indicating the deposition of metal adatoms on different termination can be a possible method to tune the work function of substrate. The deposition of Pt, Ru and Ni single atoms activates the surface N and O atoms and importantly decreases the  $|\Delta G_{\text{H}}|$  value of HER.

#### ACKNOWLEDGEMENTS

This work is financially sponsored by the National Natural Science Foundation of China (Grant No. 22372017), Liaoning Binhai Laboratory (Grant No. LBLG-2024-10), the fund of the State Key Laboratory of Catalysis in DICP (Grant No. N-22-11), and the Open Funds of State Key Laboratory of Structural Chemistry, Fujian Institute of Research on the Structure of Matter, Chinese Academy of Sciences (Grant No. 20230030).

#### REFERENCES

1. X. Chen, S. Shen, L. Guo and S. S. Mao, *Chemical Reviews*, 2010, **110**, 6503-6570.
2. Q. Wang and K. Domen, *Chemical Reviews*, 2020, **120**, 919-985.
3. Z. Wang, C. Li and K. Domen, *Chemical Society Reviews*, 2019, **48**, 2109-2125.
4. T. Hisatomi and K. Domen, *Nature Catalysis*, 2019, **2**, 387-399.
5. B. Dong, J. Cui, Y. Qi and F. Zhang, *Advanced Materials*, 2021, **33**, 2004697.
6. K. Chen, J. Xiao, T. Hisatomi and K. Domen, *Chemical Science*, 2023, **14**, 9248-9257.
7. Y. Moriya, T. Takata and K. Domen, *Coordination Chemistry Reviews*, 2013, **257**, 1957-1969.
8. A. Fuertes, *Materials Horizons*, 2015, **2**, 453-461.
9. J. Cui, C. Li and F. Zhang, *ChemSusChem*, 2019, **12**, 1872-1888.
10. N.-Y. Park and Y.-I. Kim, *Journal of Materials Science*, 2012, **47**, 5333-5340.
11. T. Watanabe, K. Tajima, J. Li, N. Matsushita and M. Yoshimura, *Chemistry Letters*, 2011, **40**, 1101-1102.
12. J. Zhou, C. Zhou, Z. Shi, Z. Xu, S. Yan and Z. Zou, *Journal of Materials Chemistry A*, 2018, **6**, 7706-7713.
13. J. J. Brown, Z. Ke, T. Ma and A. J. Page, *ChemNanoMat*, 2020, **6**, 708-719.
14. Y. Bao, H. Zou, S. Du, X. Xin, S. Wang, G. Shao and F. Zhang, *Advanced Materials*, 2023, **35**, 2302276.
15. Y. Wang, S. Jin, G. Pan, Z. Li, L. Chen, G. Liu and X. Xu, *Journal of Materials Chemistry A*, 2019, **7**, 5702-5711.
16. L. Yang, J. Yu, S. Chang and X. Xu, *Science China Materials*, 2022, **65**, 3452-3461.
17. H. Kato, K. Ueda, M. Kobayashi and M. Kakihana, *Journal of Materials Chemistry A*, 2015, **3**, 11824-11829.
18. Y. Wang, Y. Kang, H. Zhu, G. Liu, J. T. S. Irvine and X. Xu, *Advanced Science*, 2021, **8**, 2003343.
19. G. Lin, C. Zhang and X. Xu, *Journal of Materials Science & Technology*, 2023, **154**, 241-250.
20. Y. Zhang and X. Xu, *Inorganic Chemistry Frontiers*, 2021, **8**, 3723-3732.
21. R. Wang, Y. Wang, S. Chang, S. Jin, Y. Shao and X. Xu, *Journal of Catalysis*, 2020, **390**, 57-66.
22. K. Ueda, H. Kato, M. Kobayashi, M. Hara and M. Kakihana, *Journal of Materials Chemistry A*, 2013, **1**, 3667-3674.
23. M. Liu, W. You, Z. Lei, T. Tuyoshi, D. Kazunari and C. Li, *Chinese Journal of Catalysis*, 2006, **27**, 556-558.
24. L. Zhang, Y. Song, J. Feng, T. Fang, Y. Zhong, Z. Li and Z. Zou, *International Journal of Hydrogen Energy*, 2014, **39**, 7697-7704.
25. W. Si, D. Pergolesi, F. Haydous, A. Fluri, A. Wokaun and T. Lippert, *Physical Chemistry Chemical Physics*, 2017, **19**, 656-662.
26. M. Hojamberdiev, M. F. Bekheet, J. N. Hart, J. J. M. Vequizo, A. Yamakata, K. Yubuta, A. Gurlo, M. Hasegawa, K. Domen and K. Teshima, *Physical Chemistry Chemical Physics*, 2017, **19**, 22210-22220.
27. H. Huang, J. Feng, H. Fu, B. Zhang, T. Fang, Q. Qian, Y. Huang, S. Yan, J. Tang, Z. Li and Z. Zou, *Applied Catalysis B: Environmental*, 2018, **226**, 111-116.
28. X. Wang, T. Hisatomi, Z. Wang, J. Song, J. Qu, T. Takata and K. Domen, *Angewandte Chemie International Edition*, 2019, **58**, 10666-10670.
29. J. Xu, Y. Luo, Q. Guo, H. Zhou, Z. Wang and H. He, *Journal of Catalysis*, 2022, **415**, 19-27.
30. J. Yang, D. Wang, H. Han and C. Li, *Accounts of Chemical Research*, 2013, **46**, 1900-1909.
31. S. Du and F. Zhang, *Chinese Journal of Catalysis*, 2024, **61**, 1-36.
32. B. Samanta, Á. Morales-García, F. Illas, N. Goga, J. A. Anta, S. Calero, A. Bieberle-Hütter, F. Libisch, A. B. Muñoz-García, M. Pavone and M. Caspary Toroker, *Chemical Society Reviews*, 2022, **51**, 3794-3818.
33. Z.-H. Xue, D. Luan, H. Zhang and X. W. Lou, *Joule*, 2022, **6**, 92-133.
34. P. Zhou, M. Luo and S. Guo, *Nature Reviews Chemistry*, 2022, **6**, 823-838.
35. G. Kresse and J. Fürthmüller, *Physical Review B*, 1996, **54**, 11169-11186.
36. G. Kresse and J. Fürthmüller, *computational Materials Science*, 1996, **6**, 15-50.
37. P. E. Blochl, *Phys Rev B Condens Matter*, 1994, **50**, 17953-17979.
38. G. Kresse and D. Joubert, *Physical Review B*, 1999, **59**, 1758-1775.
39. J. P. Perdew and Y. Wang, *Phys Rev B Condens Matter*, 1992, **45**, 13244-13249.
40. J. P. Perdew, K. Burke and M. Ernzerhof, *Physical Review Letters*, 1996, **77**, 3865-3868.
41. S. H. Porter, Z. Huang and P. M. Woodward, *Crystal Growth & Design*, 2014, **14**, 117-125.
42. N. Cordes and W. Schnick, *Chemistry – A European Journal*, 2017, **23**, 11410-11415.
43. M. Yang, J. Oró-Solé, J. A. Rodgers, A. B. Jorge, A. Fuertes and J. P. Attfield, *Nature Chemistry*, 2011, **3**, 47-52.
44. J. P. Attfield, *Crystal Growth & Design*, 2013, **13**, 4623-4629.
45. X. Xu and H. Jiang, *Journal of Materials Chemistry A*, 2019, **7**, 14583-14591.
46. X. Xu and H. Jiang, *RSC Advances*, 2020, **10**, 24410-24418.
47. L. Clark, J. Oró-Solé, K. S. Knight, A. Fuertes and J. P. Attfield, *Chemistry of Materials*, 2013, **25**, 5004-5011.
48. A. T. Garcia-Esparza, N. Tymiąska, R. A. R. Al Orabi and T. Le Bahers, *Journal of Materials Chemistry C*, 2019, **7**, 1612-1621.
49. Y. Zhou, G. Gao, Y. Li, W. Chu and L.-W. Wang, *Physical Chemistry Chemical Physics*, 2019, **21**, 3024-3032.
50. R. Costa-Amaral and Y. Gohda, *The Journal of Chemical Physics*, 2020, **152**, 054701.
51. J. K. Nørskov, J. Rossmeisl, A. Logadottir, L. Lindqvist, J. R. Kitchin, T. Bligaard and H. Jónsson, *The Journal of Physical Chemistry B*, 2004, **108**, 17886-17892.
52. J. K. Nørskov, T. Bligaard, A. Logadottir, J. R. Kitchin, J. G. Chen, S. Pandalov and U. Stimming, *Journal of The Electrochemical Society*, 2005, **152**, 1245-1250.
53. T. B. J. K. Nørskov, A. Logadottir, J. R. Kitchin, J. G. Chen, S. Pandalov, U. Stimming, *Journal of The Electrochemical Society*, 2005, **152**, 1245-1250.

2005, **153** , J23-J26.54. J. K. Nørskov, T. Bligaard, A. Logadottir, J. R. Kitchin, J. G. Chen, S. Pandelov and U. Stimming, *Journal of The Electrochemical Society* , 2005, **152** , J23.55. T. Bligaard, J. K. Nørskov, S. Dahl, J. Matthiesen, C. H. Christensen and J. Sehested, *Journal of Catalysis* , 2004, **224** , 206-217.

#### Hosted file

image1.emf available at <https://authorea.com/users/878142/articles/1257913-theoretical-understanding-of-lataon2-decorated-with-metal-cocatalysts-for-photocatalytic-hydrogen-evolution-reaction>

**Fig. 1** Six representative *cis*-ordered structures of bulk LaTaON<sub>2</sub>. Coloring scheme: green (La), light blue (Ta), red (O) and blue (N).

#### Hosted file

image2.emf available at <https://authorea.com/users/878142/articles/1257913-theoretical-understanding-of-lataon2-decorated-with-metal-cocatalysts-for-photocatalytic-hydrogen-evolution-reaction>

**Fig. 2** Calculated band structure, density of states and charge density distributions of the VBM and CBM for bulk LaTaON<sub>2</sub>.

#### Hosted file

image3.emf available at <https://authorea.com/users/878142/articles/1257913-theoretical-understanding-of-lataon2-decorated-with-metal-cocatalysts-for-photocatalytic-hydrogen-evolution-reaction>

**Fig. 3** Top and side views of La- and Ta-terminations of LaTaON<sub>2</sub> (010) surface. The green, light blue, red and blue balls represent La, Ta, O and N atoms, respectively. The yellow circles highlight the optimized adsorption sites of metal single atoms.

#### Hosted file

image4.emf available at <https://authorea.com/users/878142/articles/1257913-theoretical-understanding-of-lataon2-decorated-with-metal-cocatalysts-for-photocatalytic-hydrogen-evolution-reaction>

**Fig. 4** Relative energies with respect to the most stable configuration of metal single atoms on the different adsorption sites of (a) La-termination and (b) Ta-termination. The adsorption sites are shown in Fig. 3.

#### Hosted file

image5.emf available at <https://authorea.com/users/878142/articles/1257913-theoretical-understanding-of-lataon2-decorated-with-metal-cocatalysts-for-photocatalytic-hydrogen-evolution-reaction>

**Fig. 5** The most stable adsorption structures of single Pt, Ru and Ni on La- and Ta-terminated (010) surface of LaTaON<sub>2</sub> attached with the corresponding adsorption energy. Coloring scheme: green (La), light blue (Ta), red (O), blue (N), grey (Pt), purple (Ru), and orange (Ni).

#### Hosted file

image6.emf available at <https://authorea.com/users/878142/articles/1257913-theoretical-understanding-of-lataon2-decorated-with-metal-cocatalysts-for-photocatalytic-hydrogen-evolution-reaction>

**Fig. 6** Partial density of states from La 5*d* , Ta 5*d*, O 2*p* , N 2*p* and M *nd* states of (a) *Pt@La* , (b) *Ru@La* , (c) *Ni@La* , (d) *Pt@Ta* , (e) *Ru@Ta* and (f) *Ni@Ta* .

#### Hosted file



image7.emf available at <https://authorea.com/users/878142/articles/1257913-theoretical-understanding-of-lataon2-decorated-with-metal-cocatalysts-for-photocatalytic-hydrogen-evolution-reaction>

**Fig. 7** Charge density differences with the isosurface value of  $0.005 \text{ e}/\text{\AA}^3$  for Pt@La, Ru@La, Ni@La, Pt@Ta, Ru@Ta and Ni@Ta. The yellow and cyan contours represent accumulation and depletion of charges, respectively.

#### Hosted file

image8.emf available at <https://authorea.com/users/878142/articles/1257913-theoretical-understanding-of-lataon2-decorated-with-metal-cocatalysts-for-photocatalytic-hydrogen-evolution-reaction>

**Fig. 8** Calculated free-energy diagram of hydrogen evolution on (a) pure surface, (b) Pt@La and Pt@Ta, (c) Ru@La and Ru@Ta, and (d) Ni@La and Ni@Ta. Varied relaxed structures and the corresponding values of  $\Delta G_{\text{H}}$  are attached. Coloring scheme: green (La), light blue (Ta), red (O), blue (N), grey (Pt), purple (Ru), orange (Ni) and white (H).